Results in Physics 14 (2019) 102383

Contents lists available at ScienceDirect

Results in Physics

journal homepage: www.elsevier.com/locate/rinp

Evaluation of anti-corrosion performance of an expired semi synthetic antibiotic cefdinir for mild steel in 1 M HCl medium: An experimental and theoretical study

Ashish Kumar Singh[a,*], Bhawna Chugh[b], Sourav Kr. Saha[c,1], Priyabrata Banerjee[c], Eno E. Ebenso[d], Sanjeeve Thakur[b], Balaram Pani[e]

[a] Department of Applied Science, BharatiVidyapeeth's College of Engineering, New Delhi 110063, India
[b] Department of Chemistry, Netaji Subhash Institute of Technology, New Delhi 110078, India
[c] Surface Engineering & Tribology Group, CSIR-Central Mechanical Engineering Research Institute, Mahatma Gandhi Avenue, Durgapur 713209, West Bengal, India
[d] Material Science Innovation & Modelling (MaSIM) Research Focus Area, Faculty of Natural and Agricultural Sciences, North-WestUniversity, Private Bag X2046, Mmabatho 2735, South Africa
[e] Department of Chemistry, Bhaskaracharya College of Applied Science, University of Delhi, New Delhi 110078, India

ARTICLE INFO

Keywords:
Adsorption
Electrochemistry
Activation parameters
DFT
MD simulation

ABSTRACT

In view of severity of metallic corrosion in different corrosive media, application of corrosion inhibitor has been very promising to overcome this problem. However, numbers of corrosion inhibitors investigated earlier are not environmentally safe as well as costlier. To overcome these problems, researches are going on to develop efficient, environment friendly as well as cost effective corrosion inhibitor. In view of these facts, corrosion inhibition property of an expired anti-biotic, cefdinir (CDR) was investigated. This study includes anti-corrosion performance of CDR molecule against corrosion of mild steel (MS) in HCl medium. The results are summarized on the basis of weight loss, electrochemical, morphological and theoretical studies. The weight loss study infers that the rate of corrosion regularly decreased by the increasing the amount of CDR in acid solution. The cefdinir thus adsorbed on the MS surface and mitigate the corrosion rate. The adsorption of CDR on MS surface obeys Langmuir isotherm. The activation energy regularly increased by the presence of CDR and hence indicated that energy barrier for corrosion process to take place increased. The increased entropy of activation in presence of CDR assigned to entropy of solvent molecule. Potentiodynamic study infers that the CDR acts as mixed type of inhibitor. The value of Gibb's free energy suggested the electrostatic as well as chemical interaction of CDR molecule with mild steel surface. The theoretical study (Density functional theory, Fukui indices and Molecular dynamics) justifies the experimental results appreciably.

Introduction

Metals have ever been important for our life. The different metallic properties, hardness, ductility, rigidity, strength, high resistance against natural wear and tear make the way for variety of uses of metals. Metals have been used by man in various forms since ancient time or better to speak since evolution. Not only our body needs metals like Cu & Zn for its proper functioning [1] but also number of amenities in life would not exist. Generally all the metals are thermodynamically unstable and hence tend to revert in their stable state by reacting with their environment. This forms the basic cause of metallic corrosion. The metallic corrosion results in to economic loss and may lead to safety and health issues of industry workers as well as peoples residing in nearby towns. Due to their high sensitivity against different corrosive environments as well as their importance for human society metals need to be protected from corrosion.

Due to cost-effectiveness and appreciable mechanical strength, mild steel is considered as one of the most commonly used steel. It is widely used in number of industries such as pipelines, buildings; bridges and tin cans [1].The mild steel is exposed to different corrosive atmosphere in these industries and hence corrodes easily. Thus, protection of mild steel from corrosion has ever been felt. The application of inhibitors is

* Corresponding author.
E-mail address: ashish.singh.rs.apc@itbhu.ac.in (A.K. Singh).
[1] Present address: Department of Nuclear and Quantum Engineering, Korea Advanced Institute of Science and Technology, 373-1 Guseong, Yuseong, Daejeon, 305-701, Republic of Korea.

https://doi.org/10.1016/j.rinp.2019.102383
Received 3 April 2019; Received in revised form 23 May 2019; Accepted 23 May 2019
Available online 29 May 2019

one of the most primitive methods of corrosion control and has been very promising, cost-effective [2–5]. The inhibitors interact with the metal surface and thereby adsorbed them self on the metallic surface. The chemical structure of an inhibitor is closely related to its adsorption ability. Earlier studies have reported that organic compounds having hetero atoms, conjugated π-bonds and aromatic nucleus show appreciable efficiency to mitigate [6–10]. Thus, keeping this in view, hetero-aromatic compounds have been widely studied as corrosion inhibitor because of having greater tendency to form metallic complex with metal ions because of having either non-bonding electrons or sometimes having vacant d-orbital (in case of S-compounds). The toxic nature of these compounds led the Corrosion Scientists to think about the development of non-hazardous and environment friendly inhibitors [11–12].

In the light of the development of non-hazardous, environmentally benign inhibitors, corrosion inhibition property of various drugs in different corrosive medium has been studied [13–19]. Moreover the importance of cost effective drugs for illness of poor people's led researchers to study some expired drugs as corrosion inhibitor to protect metal from corrosion in various corrosive environments [20–22]. The use of expired drug as corrosion inhibitor solves our environmental problem also as their disposal imposes a problem before us. These problems led us to study anti-corrosion property of an expired Cefdinir. In this paper, anticorrosion property of cefdinir (CDR) against acidic corrosion of mild steel is reported. Cefdinir is an antibiotic of third generation of Cephalosporin. The chemical structure and IR spectrum of cefdinir is presented as Fig. 1.

The selection of expired cefdinir was made due to its size as it is big enough to cover the mild steel surface effectively to retard the corrosion as well as it solve some other problems also as (i) It would be economical as the use of expired drug ruled out its disposal cost and (ii) it would reduce environmental pollution because of its application as corrosion inhibitor.

Recently, theoretical study has been emerged as an important tool to determine the relationship between structure and activity [23–24]. To examine the effect of molecular structure and different orientations on anticorrosion potential of CDR, density functional theory (DFT) calculations were done. For this purpose ORCA programme package (version 2.7.0) [25] was used and geometry optimization was achieved by B3LYP functional level of DFT [26–30]. Gaussian basis set was used in this study which was developed by the Ahlrich's group [31].

Atomic force microscopy (AFM) being an important tool for surface study was used to study the effect of CDR on metal surface. The hydrophobicity of acid solution containing CDR is studied by contact angle measurement.

The corrosion mitigating potential of CDR was further compared with some earlier studied drug molecule as corrosion inhibitor for mild steel in acid medium. The comparative corrosion mitigating efficiency data are provided in Table 1. The optimum concentration of CDR used in this study was 5.05×10^{-4} M (200 ppm), while the concentrations of earlier reported drug molecules were ranging from 500 to 1266 ppm. Thus, the results obtained have proven CDR as an excellent corrosion inhibitor at low concentration. Also, the use expired drug, CDR, offer cost effective solution for corrosion mitigation.

Table 1
Inhibition efficiency values of CDR showing supremacy with some other studied inhibitors.

Name of Inhibitor	Optimum Conc./Mg l^{-1}	E_{WL}%
Cefdinir/CDR	$200/5.05 \times 10^{-4}$ M	97
Cefotaxime Sodium	500	95
Doxycycline	500	94
Cefazolin	500	94
Streptomycin	500	88
Sulphadiazine	1200	94
Sulphamethaxazole	1266	93
Cefalexin	500	92
Ceftobiprole	500	92

Experimental procedure

Preparation of metal sample

Mild steel samples used for this study were cut in to size $2.5 \times 2.0 \times 0.025\,cm^3$ for weight loss experiments and $7.5 \times 1.0 \times 0.025\,cm^3$ for electrochemical experiments respectively. These samples were abraded, washed thoroughly, dried and then used to perform experiments. The composition and density of mild steel used in this study was determined and is presentedas Table 2.

The mild steel coupons used to scan atomic force micrographs were prepared similarly. The inhibitor solution was made in 1 M HCl. Hydrochloric acid and ethanol were mixed in 9:1 ratio just ensure the solubility of CDR molecule. The analytical grade HCl (37%) was used to prepare stock acid solution which was further used to study anti-corrosion performance of CDR; the spectral details of CDR molecule is presented as:

FT-IR (KBr, cm^{-1}): 3286 (NH stretching); 2918, 2851 (CH stretching); 1767 {CO stretching (COOH)}; 1665 {CO stretching (CONH)}; 1585 (NH out of plane); 1336 (CN stretching-aromatic); 992 (=CH out of plane); 799 (CH bending)

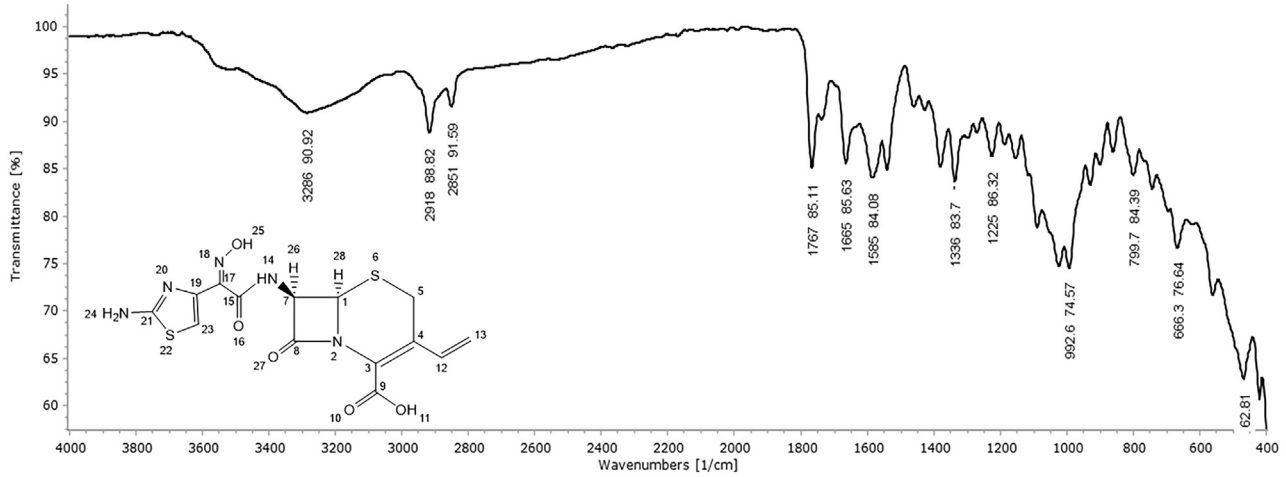

Fig. 1. Molecular structure of Cefdinir (CDR).

Table 2
Composition and density of tested mild steel sample.

Density (g cm^{-3})	Composition	
	Elements	% (by weight)
7.87	C	0.17
	Mn	0.46
	Si	0.26
	S	0.01
	P	0.02
	Fe	99.07

Electrochemical measurements

To analyze the corrosion inhibiting potential of CDR, electrochemical experiments; EIS and potentiodynamic potential were run. The concentrated solution of CDR was prepared in 1 M HCl and this solution was diluted up to different concentrations to run electrochemical experiments separately. The counter electrode consists of Pt foil ($1 \times 1\ cm^2$) and saturated calomel (SC) works as reference one while working electrode consists of mild steel. Before running electrochemical experiments the working electrodes were dipped in solution with different concentrations of CDR for 30 min to stabilize the corrosion potential.

The Potentiostat/Galvanostat used to run electrochemical experiments was supplied from Gamry; model 300 [32]. This electrochemical work station fitted with software Echem analyst to check the fitting of all the experimental data with an appropriate equivalent circuit.

Potentiodynamic polarization experiments were run in the + 250 to − 250 mV potential range with scan rate 1 mV s^{-1}.

Gravimetric experiments

These experiments were performed according to ASTM G31 standard [33]. The molar HCl solutions with different CDR strength were prepared and mild steel samples were dipped in it for 3 h. After 3 h weight loss data were calculated by weighing these mild steel specimens.

Evaluation of wetting behaviour

The wetting behaviour of metal surface becomes so important and has attracted considerable interest from both fundamental as well as application point of view. The solid-liquid wettability considerably affects anticorrosion performance of an inhibitor. DSA Kruss optical contact angle measurement instrument based on sessile drop technique, made in Germany, was used to measure contact angle by the method as described elsewhere [34]. The mild steel coupons were thoroughly cleaned to assure no contaminant present on its surface to perform contact angle measurement experiment. The acid solutions having varying concentrations of CDR are then placed as drop on the MS surface and measured the contact angle.

Theoretical study

Quantum chemical calculation

Generally corrosion inhibitor must be adsorbed on the desired metallic surface to show corrosion inhibiting potential. Basically, it is the electronic properties and molecular structure of corrosion inhibitor which affect their adsorption on any surface. In this connection, DFT has been proved an important tool to optimize the structure of inhibitors and also to get their electronic properties. ORCA programme package [25] was the source to ensure DFT calculations and B3LYP functional level of DFT [26–30] to get optimize geometry of CDR molecule. Ahlrich's group [31] developed all-electron Gaussian basis set was used to perform this study. Triple-ζ quality basis set together with a set of polarisation functions were used for N & O atoms while polarized split valence and a polarizing set of d functions were used for C & H and non-hydrogen atoms respectively in this study. In this analysis, solvent effect is also considered because of the fact that liquid medium is necessary to occur this type of corrosion. Herein, effect of solvent (here water) has been introduced by the utilization of COSMO model during the optimization process.

Analysis of reactive sites which are responsible for adsorption was accomplished by Fukui Indices (FIs). The software used to get FIs of all the atoms of CDR molecule was Material studio™ 6.1 versions [35] with DMol3 module. Application of double numerical polarization combined together with generalized gradient approximation and BLYP exchange correlation functional [36,37] was required to calculate all the FIs. The condensed Fukui function gives the detailed information of the local reactive centres of the inhibitor molecules. The Fukui function (f_x) can be defined as [38]:

$$f_x = \left(\frac{\partial \rho(\vec{r})}{\partial Y}\right)_{\upsilon(\vec{r})} \tag{1}$$

where, $\rho(\vec{r})$, Y and $\upsilon(\vec{r})$ are first derivative of electron density, number of electrons and constant external potential respectively.

With the help of finite difference approximations, Fukui functions can be determined for nucleophilic and electrophilic attacks by inhibitor molecule separately as follows [39]:

For Nucleophilic attack

$$f_x^- = q_x(Y+1) - q_x(Y) \tag{2}$$

And for electrophilic attack

$$f_x^- = q_x(Y) - q_x(Y-1) \tag{3}$$

where, q_x represents total charge of the x atom, while $q_x(Y+1)$stands for charge of the anionic form, $q_x(Y)$ for neutral form and $q_x(Y-1)$ for cationic form of x atom respectively. Hirshfeld population analysis, i.e. HPA represented Fukui functions in this study.

Molecular dynamics study

It is well established fact that inhibitors interact with the metal surface to be adsorbed and this interaction can be easily predicted by molecular dynamics, i.e. MD simulation technique. To carry out simulation study, Fe (1 1 0) surface is selected because of packed surface and high stabilization energy. The interaction of CDR molecule with the metallic surfaces has been modelled in a 3D simulation box (dimension: $39.96 \times 39.96 \times 77.61$ Å). The whole simulation box has been constructed of three layers which includes first layer consists of a layer of Fe block followed by 10 subsequent layers of Fe atoms, second layer which is the solution block consisting of inhibitor molecule, H_2O molecules and molecular ions like H_3O^+ and Cl^- and the third one the last uppermost vacuum layer. In this case, COMPASS, i.e. Condensed Phase Optimized Molecular Potentials for Atomistic Simulation Studies which is highly accepted has been used. COMPASS, an originally force field provides accurate prediction about chemical properties of a molecule/s [40]. The COMPASS force field can be defined as [29,41–43]:

$$E = E_{bs} + E_{ab} + E_{opac} + E_{torsion} + E_{cc} + E_{elec} + E_{VB} \tag{4}$$

where E_{bs}, E_{ab}, E_{opac}, $E_{torsion}$, E_{cc}, E_{elec} and E_{VB} stands for contribution due to bond stretching, due to angle bending, due to out of plane angle coordinates, due to torsion, due to cross coupling, due to electrostatic and due to Vander Waals interaction respectively. All the terms of Eq. 4can be written separately as:

$$E_{bs} = \sum_b [x_2(b-b_0)^2 + x_3(b-b_0)^3 + x_4(b-b_0)^4] \tag{5}$$

$$E_{ab} = \sum_\theta [H_2(\theta-\theta_0)^2 + H_3(\theta-\theta_0)^3 + H_4(\theta-\theta_0)^4] \tag{6}$$

$$E_{\text{torsion}} = \sum_{\phi} [V_1[1 - \cos(\phi - \phi_0)^2] + V_2[1 - \cos(2\phi - \phi_0)^2] + V_3 [1 - \cos(3\phi - \phi_0)^2]] \quad (7)$$

$$E_{\text{opac}} = \sum_{\chi} x_{\chi}\chi^2 \quad (8)$$

$$E_{cc} = \sum_b \sum_{b'} F_{bb'}(b - b_0)(b' - b_0') + \sum_{\theta} \sum_{\theta'} F_{\theta\theta'}(\theta - \theta_0)(\theta' - \theta_0') + \sum_b \sum_{\theta} F_{b\theta}(b - b_0)(\theta - \theta_0) + \sum_b \sum_{\phi} F_{b\varphi}(b - b_0)[V_1 \cos\phi + V_2 \cos 2\phi + V_3 \cos 3\phi] + \sum_{b'} \sum_{\phi} F_{b'\varphi}(b' - b_0')[V_1 \cos\phi + V_2 \cos 2\phi + V_3 \cos 3\phi] + \sum_{\theta} \sum_{\phi} F_{\theta\varphi}(\theta - \theta_0)[V_1 \cos\phi + V_2 \cos 2\phi + V_3 \cos 3\phi] + \sum_{\theta} \sum_{\theta'} \sum_{\phi} k_{\varphi\theta\theta'} \cos\phi(\theta - \theta_0)(\theta' - \theta_0') \quad (9)$$

$$E_{\text{elec}} = \sum_{i.j} \frac{q_i q_j}{\varepsilon r_{ij}} \quad (10)$$

$$E_{\text{VB}} = \sum_{i.j} \varepsilon_{ij} \left[2\left(\frac{r_{ij}^0}{r_{ij}}\right)^9 - 3\left(\frac{r_{ij}^0}{r_{ij}}\right)^6 \right] \quad (11)$$

where, b, θ, ϕ and χ stands for bond length, bond angle, angle of torsion and out of plane angle respectively.

During entire simulation study, Fe atoms are kept static while all remaining species involved in simulation are allow to interact freely with the metallic surfaces. In this study, MD simulations run by incorporating NVT canonical ensemble at 298 K temperature with 1 fs time step and 100 ps simulation period.

The total energy of interaction (E_{inter}) due to interaction inhibitor molecule with Fe surface can easily be derived as [29,30]:

$$E_{\text{inter}} = E_{\text{total}} - \left(E_{\text{surf} + H_2O + H_3O^+ + Cl^-} + E_{\text{inh}}\right) \quad (12)$$

where, E_{total}, E_{inh}, and $E_{\text{surf} + H_2O + H_3O^+ + Cl^-}$ represents total energy of the whole simulation system, energy of adsorption inhibitor and energy of metallic surface and all other concerned species like H_2O, H_3O^+ and Cl^-.

The negative of interaction energy can be taken as binding energy of the inhibitor as:

$$E_{\text{binding}} = -E_{\text{inter}} \quad (13)$$

Surface study; atomic force microscopy (AFM)

The topographical study of mild steel samples was carried out by scanning atomic force micrographs. The mild steel samples were prepared in the same way as in the TGA experiment to run scan AFM images. NT-MDT multimode AFM was used to scan the topographical images. This instrument was supplied from Russia. The AFM was run in semi-contact mode [44] to record micrographs of mild steel surface.

Results and discussion

Electrochemical impedance spectroscopic data

Table 3 represented the results obtained by running EIS with different solutions of CDR in molar hydrochloric acid. The performance of CDR against corrosion of mild steel corrosion acid is shown as Nyquist and Bode-Phase plots and represented as Fig. 2a–c.

The Nyquist plots obtained consist of two loops; large capacitive loop and small inductive loop. The capacitive obtained at higher frequency and contributed significantly to reduce the corrosion rate while inductive loop obtained at lower frequency. The inhibiting action of an inhibitor is a function of diameter of Nyquist plot; greater the diameter of Nyquist plot, greater will be its efficiency. The performance of CDR to reduce corrosion bettered by increasing its amount in HCl acid solution as confirmed by increased diameter of Nyquist plots which indicated adsorption of CDR over metal surface. The high frequency capacitive loop was formed due to charge transfer process occurred on the studied surface while relaxation of corrosion products and/or adsorption of CDR accounted for the formation of low frequency inductive loop. The size of inductive loop increased appreciably at higher concentrations of CDR and thus confirmed its adsorption and thereby corrosion rate is reduced. The surface state may have short or long relaxation time which is defines as [45–47]

$$\tau = CR_{ct} \quad (14)$$

where, C is used for capacitance while R_{ct} for resistance due to charge transfer, i.e. charge transfer resistance. Thus, higher values of charge transfer resistance at higher concentration of CDR resulted into longer relaxation time. The values of relaxation time presented in the Table 3.

The phase angle at intermediate frequency measures the capacitive behaviour of electrode. The phase angle increased by the increase in CDR concentration indicates the more capacitive behaviour or effective control of corrosion at higher concentrations of CDR.

The charge transfer resistance (R_{ct}) can be used to analyse anti-corrosion performance of CDR as:

$$E_{R_{ct}}\% = \frac{R_{ct}^i - R_{ct}^0}{R_{ct}^i} \times 100 \quad (15)$$

where, R_{ct}^i stands for charge transfer resistance with inhibitor while R_{ct}^0 for the same in without inhibitor.

The Nyquist plots obtained is depressed semicircle instead of perfect semicircle and this depression is characteristically associated with heterogeneity of electrode which can be explained by incorporating constant phase element in equivalent circuit.

An equivalent circuit used to fit all the experimental data of EIS is presented as Fig. 2d. This equivalent circuit includes modification in the form of CPE for double layer capacitance and consists of parallel combination of R_{ct} and *CPE* connected in series to a parallel combination of inductive element (L) and inductive resistance $R_{L.}$ The value of inductance, L, is a function of inhibitor concentration as its value decreased by increasing concentration of inhibitor shown in Table 3. The decreasing value of L indicated increasing adsorption of CDR over the metal surface.

The value of n is closely related to roughness of electrode surface. The value of n increased by the presence of increasing amount of CDR (Table 3) and thus confirmed reduced corrosion and also surface roughness.

Potentiodynamic polarization

Potentiodynamic polarization experiments were conducted at different temperature (308–338 K) in acid solutions having different amount of CDR to derive information about kinetics of corrosion inhibition mechanism. The increment of corrosion current density at higher temperatures indicates that equilibrium is shifted towards desorption at higher temperatures. The Fig. 3 presented polarization curves obtained after running the experiment with different amount of CDR at temperature range 308–338 K. Addition of CDR to the acid solution lowered the corrosion current density and hence corrosion inhibition efficiency of CDR is confirmed. The corrosion potential shifted insignificantly (2–22 mV) by the presence of different concentrations of CDR which confirmed its mixed type nature. Similar findings reported by some other researchers [48,49].

The corrosion mitigating potential of CDR can be calculated from the data of potentiodynamic polarization experiments as

Table 3
Impedance parameters for mild steel in 1 M HCl in absence and presence of different concentrations of CDR at 308.

Conc. of inhibitor ($M \times 10^{-4}$)	R_s ($\Omega\ cm^2$)	Y_0 ($10^{-6} \times \Omega^{-1}\ s^n\ cm^{-2}$)	n	L (H)	R_{ct} ($\Omega\ cm^2$)	R_L ($\Omega\ cm^2$)	τ (s)	$E_{R_{ct}}$%
–	1.30	164.0	0.811	13.0	16.0	1.0	0.0006	–
0.63	0.95	75.2	0.835	12.2	84.2	5.6	0.0020	81.1
1.26	0.74	66.2	0.862	10.1	100.9	11.4	0.0020	84.8
2.52	1.09	50.9	0.863	9.3	120.0	12.8	0.0030	87.2
3.79	1.10	45.8	0.899	8.5	188.2	11.4	0.0050	91.5
5.05	1.04	20.5	0.902	7.6	485.3	55.8	0.0090	96.8
6.32	1.07	18.8	0.903	6.7	514.0	28.8	0.0058	96.9

$$E_{PDP}\% = \frac{i^0_{corr} - i^i_{corr}}{i^0_{corr}} \times 100 \quad (16)$$

where, i^0_{corr} stands for corrosion current density in 1 M HCl and i^i_{corr} stands for corrosion current density in presence of CDR.

Polarization curves were analysed by Tafel fit and obtained different parameters are listed in Table 4.

The decrease of inhibition efficiency of CDR at higher temperatures confirmed the shift of equilibrium towards desorption at higher temperatures. The values of anodic Tafel constant b_a are somewhat constant while the value of cathodic Tafel slope b_c was changed by the presence of different concentration of CDR which confirmed predominant cathodic nature of CDR.

The results of EIS as well as potentiodynamic polarization study showed consistency up to an appreciable extent.

Gravimetrical analysis

Assessment of corrosion inhibition

The relation of corrosion rate with CDR concentration and time up to which mild steel samples were immersed are presented as Fig. 4a & b respectively. The linear increase of corrosion inhibition potential of CDR by increase of its concentration resulted due to its increased adsorption. The continuous decrease of weight loss for a particular immersion period at higher concentration of CDR (Fig. 4b) confirms the stability of CDR film formed due to its adsorption. The gravimetric and electrochemical results agreed well as seen in Table 5.

Temperature study

To investigate the corrosion inhibiting potential of CDR at higher temperatures, gravimetrical analyses were carried out with different amount of CDR at different temperatures in the temperature range 308–338 K and the result is presented as Fig. 4c. The decreased efficiency of CDR at higher temperatures is due to shifting of adsorption-desorption equilibrium towards desorption.

Thermodynamic activation parameters

The temperature studies have been proved very important as it provides information regarding reaction kinetics of corrosion process. The adsorption-desorption equilibrium changed by the change in temperature and therefore interaction of CDR with mild steel surface changed also at different temperatures. Thus, to explain reaction kinetics of corrosion inhibition, potentiodynamic polarizations as well as gravimetrical analysis were carried out at different temperatures in the temperature range 308–338 K with different amount of CDR. The results obtained from both studies agreed well.

The activation parameters can be calculated using following relations [50]:

$$\log(C_R) = \frac{-E_a}{2.303RT} + \log\lambda \quad (17)$$

$$C_R = \frac{RT}{Nh}\exp\left(\frac{\Delta S^*}{R}\right)\exp\left(-\frac{\Delta H^*}{RT}\right) \quad (18)$$

where, E_a stands for activation energy, λ for Arrhenius factor, ΔH^* for

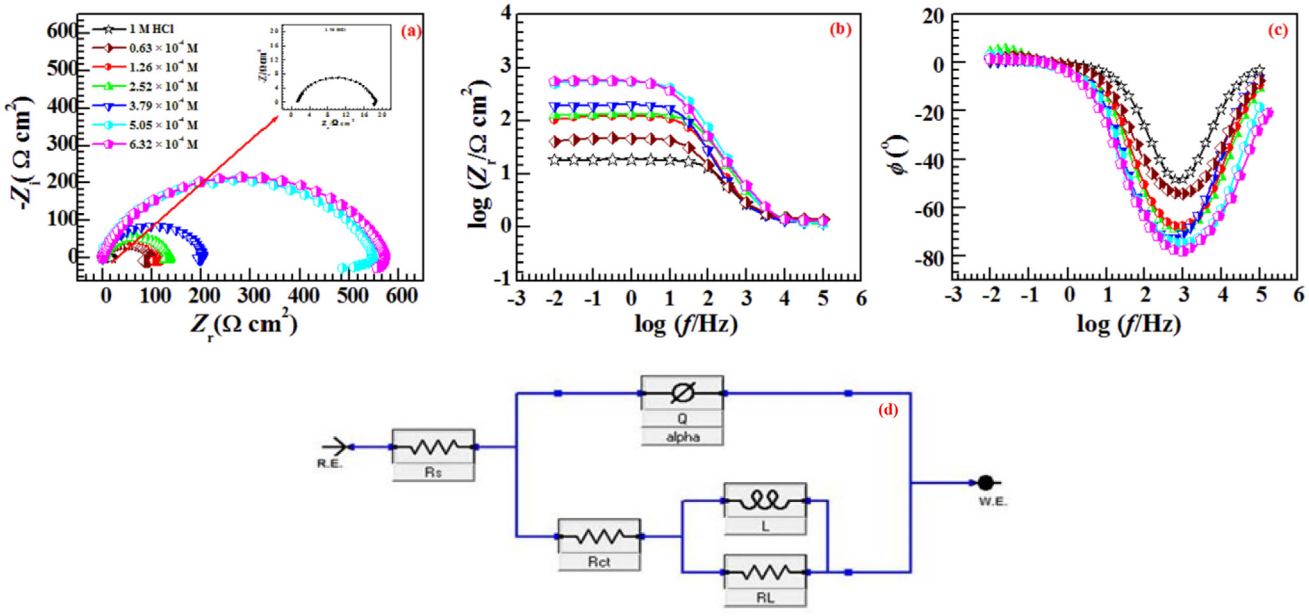

Fig. 2. (a) Nyquist plot, (b) Bode-magnitude plot and (c) Phase angle plots obtained for the mild steel in 1 M HCl in the absence and presence of different concentrations of CDR and (d) The electrochemical equivalent circuit used to fit the impedance measurement.

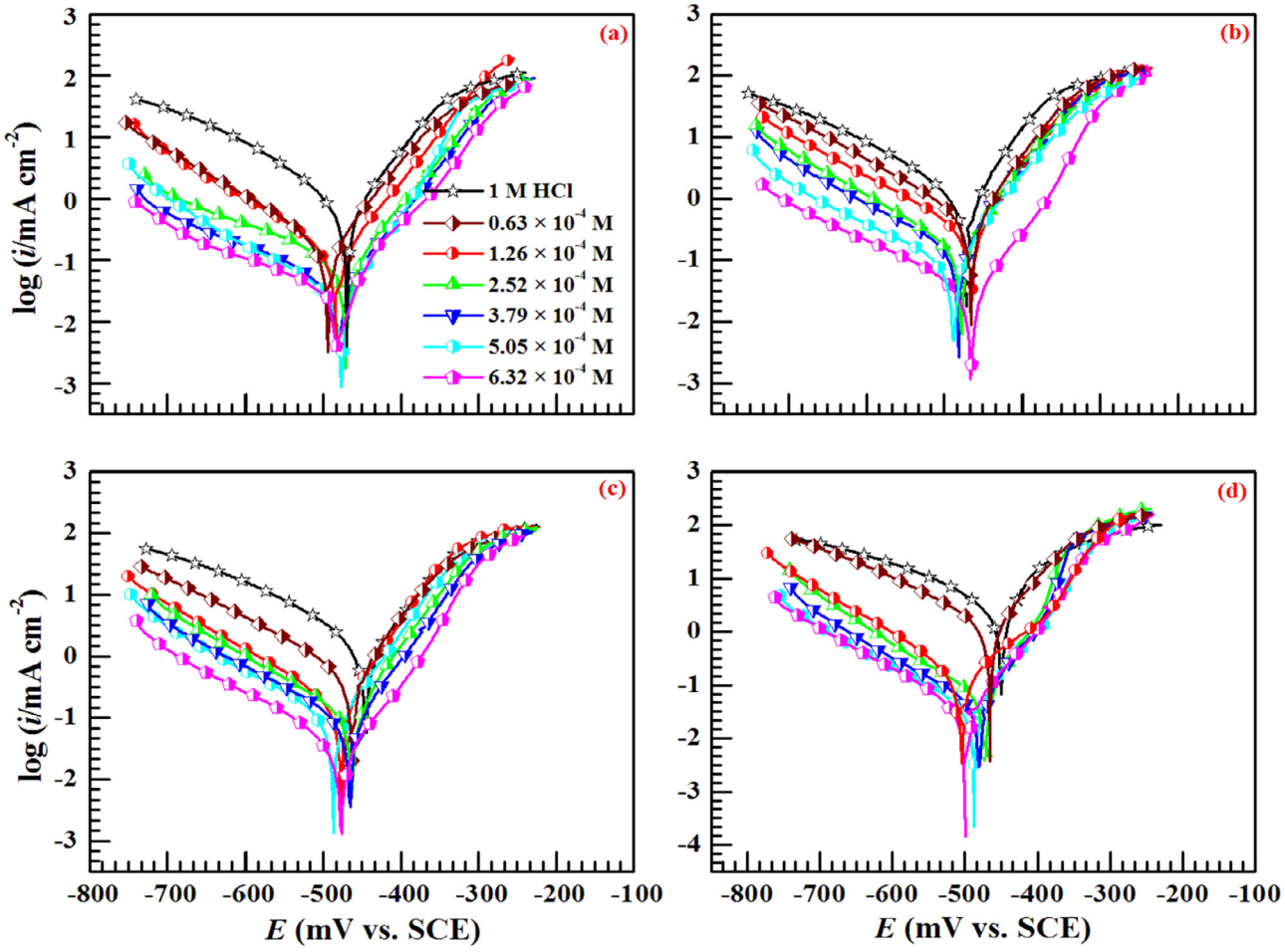

Fig. 3. Tafel Polarization curves for corrosion of mild steel in 1 M HCl medium in absence and presence of different concentrations of CDR at (a) 308 K, (b) 318 K, (c) 328 K and (d) 338 K.

Table 4
Potentiodynamic polarization parameters for mild steel without and with different concentrations of CDR in 1 M HCl at 308 K.

Conc. Of Inhibitor ($M \times 10^{-4}$)	$-E_{corr}$ (mV *vs.* SCE)	i_{corr} ($\mu A\ cm^{-2}$)	b_a (mV dec^{-1})	b_c (mV dec^{-1})	E_{PDP}%
–	469	730	73	127	–
0.63	482	184	72	135	74.8
1.26	462	131	72	132	82.0
2.52	471	112	75	181	84.6
3.79	469	55	80	154	92.4
5.05	476	35	76	184	95.2
6.32	481	32	77	168	95.6

activation enthalpy, ΔS^* for activation entropy, h for Planck's constant and N for Avogadro number, respectively. These activation parameters listed in Table 6 were calculated from slope and intercept of the graphs $\log C_R$ *vs.* $1/T$ and $\log (C_R/T)$ against $1/T$ presented as Fig. 5a-b.

The increased activation energy of corrosion process by the presence of CDR revealed that higher energy barrier to be crossed for corrosion to occur.

According to Eq. (17), the value of E_a and λ both can affect the corrosion rate. According to Eqn17, higher values of activation energy and lower values of pre-exponential factor favours lower corrosion rate. The examination of Table 6 reveals that values of both E_a and λ increased by increase in CDR concentration; thus, it is the increase in activation energy which controls corrosion rate.

The higher values of ΔH^* in inhibited solution attributed to high corrosion inhibiting potential of CDR; similar findings reported earlier [51].

As we can observe the values of ΔS^*increased in presence of CDR (Table 6) as compared to uninhibited solution which indicated that the entropy of solvent, i.e. water increased in the adsorption-desorption equilibrium.

Adsorption isotherm

The interaction of organic compounds and metal surface is of two types; physical (through electrostatic force of attraction or simple Wander Waals force of attraction) and chemical (through chemical bonds). This interaction of organic compounds mainly depends on nature of metal, chemical structure of inhibitor molecule which is to be adsorbed and electrolyte medium. When metal is immersed in inhibited acid solution, inhibitor molecules started to adsorb competitively on the metal surface. Thus, equilibrium is established between adsorbed CDR molecule and CDR molecules remained in the bulk of the acid solution. This equilibrium can be described by adsorption isotherm. When mild steel sample, i.e. working electrode immersed in electrolytic solution, an organo-electrochemical reaction occurred on its surface and the mechanism of such reaction can be explained by the application of appropriate adsorption isotherm. A variety of adsorption isotherms were examined to explain the adsorption of CDR molecule over the electrode surface in best way; this purpose served best by applying Langmuir isotherm as presented by Fig. 6a-b. This isotherm can be defined as:

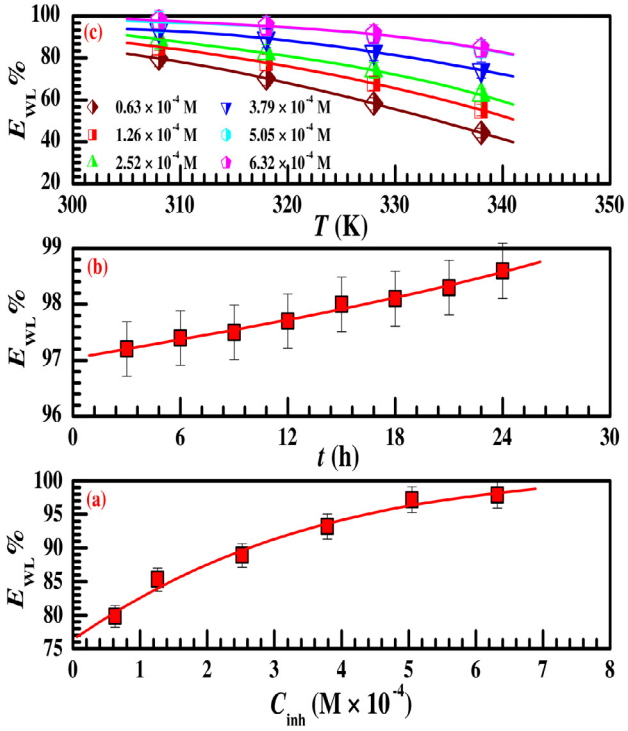

Fig. 4. Performance of CDR against (a) inhibitor conc., (b) immersion time and (c) temperature.

Table 5
Inhibition Efficiency of CDR obtained from different methods at 308 K.

Conc. Of Inhibitor	Inhibition Efficiency		
($M \times 10^{-4}$)	E_{Rct}%	E_{PDP}%	E_{WL}%
0.63	81.1	74.8	79.8
1.26	84.8	82.0	85.3
2.52	87.2	84.6	88.9
3.79	91.5	92.4	93.2
5.05	96.8	95.2	97.2
6.32	96.9	95.6	97.9

$$\theta = \frac{K_{ads}C_{inh}}{1 + K_{ads}C_{inh}} \quad (19)$$

where, K_{ads} is the adsorption constant measures the strength of adsorption. This Eqn can also be written as

$$\frac{C_{inh}}{\theta} = \frac{1}{K_{ads}} + C_{inh} \quad (20)$$

The value of K_{ads} is a function of adsorption strength of inhibitor CDR to the metal surface [52]. The appreciable inhibition potential of CDR is in accordance with high values of adsorption constant K_{ads}.

The adsorption constant K_{ads} is related to Gibb's free energy of adsorption as

$$\log K_{ads} = -\log C_{H_2O} - \frac{\Delta G^o_{ads}}{2.303RT} \quad (21)$$

where, C_{H_2O}, R and T stands for concentration of water in the taken solution in mol L^{-1}, gas constant and absolute temperature respectively.

According to Van't Hoff Eq. [53]:

$$\ln K_{ads} = \frac{1}{55.5} + \frac{-\Delta H_{ads}}{RT} + \frac{\Delta S_{ads}}{R} \quad (22)$$

The plots of $\ln K_{ads}$ (obtained from weight loss as well as polarization study) *vs.*$1/T$ presented as Fig. 6c&d. The slope and intercept of these plots provided the value of enthalpy (ΔH^o_{ads}) and entropy of adsorption (ΔS^o_{ads}) which are listed in Table 7.

The Gibb's Helmholtz Eqn can also be used to derive the value of ΔH^o_{ads} and ΔS^o_{ads} as:

$$\Delta G^o_{ads} = \Delta H^o_{ads} - T\Delta S^o_{ads} \quad (23)$$

The plot of ΔG^o_{ads} *vs.*T (presented as Fig. 6e&f) provided the value of ΔS^o_{ads} and ΔH^o_{ads} from slope and intercept respectively.

The values of thermodynamic adsorption parameters obtained from different methods showed appreciable consistency. In this study the value of ΔH^o_{ads} is negative and the value of ΔS^o_{ads} is positive as listed in Table 7. Thus it is the increasing entropy resulted in negative value of Gibb's free energy of adsorption. Hence, the driven force for adsorption was entropy not enthalpy, as reported elsewhere [54].

Contact angle analysis (Wetting interaction between acid solution and mild steel surface)

The contact angle is a function of interaction between solution and the metal surface. The measurement of contact angle was performed for acid solutions with varying CDR strength and the result presented as Fig. 7. The value of contact angle decreased continuously by the presence of increasing amount of CDR and thus confirmed the potential of CDR molecule to reduce the interaction of mild steel with acid solution. Thus, potential of CDR to inhibit corrosion increased with its concentration. Solmaz et al. [55] reported similar findings in their report.

Theoretical study

Quantum chemical calculations of the neutral form of inhibitor molecule

Quantum chemical calculation eased the designing and development of efficient corrosion inhibitors recently. DFT study explores all the possible D-A interaction at the level of each and every atoms of inhibitor molecule. It is widely studied fact that for a molecule should be adsorbed to show corrosion inhibition property and it is mainly the D-A type interaction which is responsible for adsorption over the preferred surface. Thus DFT offered the relationship of molecular structure or properties with corrosion inhibiting capability of a molecule. Based on this fact quantum chemical calculation has been accomplished to

Table 6
Calculated values of activation parameters for mild steel in 1 M HCl in the absence and presence of different concentrations of CDR.

Conc. of Inhibitor	E_a (KJ mol^{-1})		ΔH^* (kJ mol^{-1})		ΔS^* (J mol^{-1} K^{-1})		λ (mg cm^{-2})	
($M \times 10^{-4}$)	WL	PDP	WL	PDP	WL	PDP	WL	PDP
–	42.21	36.37	39.55	33.73	−86.75	−94.99	5.31×10^8	1.98×10^8
0.63	71.23	61.89	64.58	59.38	−24.99	−26.74	8.95×10^{11}	7.27×10^{11}
1.26	74.02	64.37	71.37	61.70	−18.62	−15.26	19.27×10^{11}	2.89×10^{12}
2.52	76.57	68.17	73.92	65.61	−12.63	−14.31	39.62×10^{11}	3.24×10^{12}
3.79	80.58	76.34	77.93	73.75	−3.95	−10.19	11.27×10^{12}	6.17×10^{13}
5.05	91.24	85.34	88.58	82.73	23.10	−15.67	29.24×10^{13}	25.8×10^{13}
6.32	98.52	91.56	95.87	88.92	44.96	−25.73	40.55×10^{14}	36.1×10^{14}

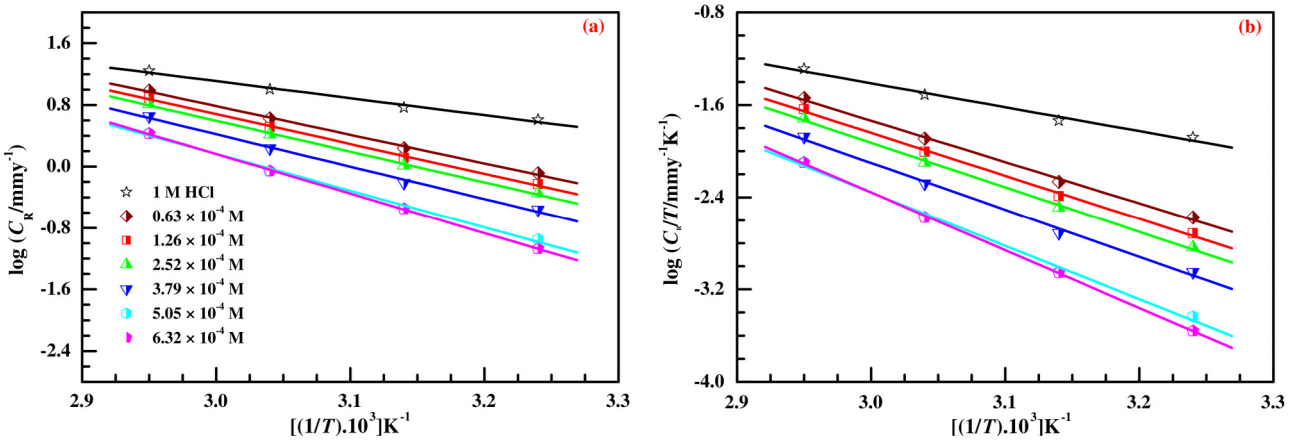

Fig. 5. (a) Arrhenius plot of log CR *vs.* 1/T in absence and presence of different concentrations of CDR and (b) log (CR/T) *vs.* 1/T in absence and presence of different concentrations of CDR obtained from weight loss measurements.

explain the corrosion inhibition mechanism of CDR over mild steel surface. The optimized geometry structure, electron density distribution over the highest occupied and lowest unoccupied molecular orbital i.e. HOMO and LUMO of CDR molecule are presented in Fig. 8a–c. Several quantum chemical parameters obtained from DFT calculations such as energy of frontier molecular orbitals (E_{HOMO} and E_{LUMO}), energy gap (ΔE), dipole moment (μ), electronegativity (χ), hardness (η), Softness (S) and fraction of electron transferred (ΔY) listed Table 8.

The frontier molecular orbitals (FMO's) theory states that chemical reactivity of a molecule is primarily depends on optimized geometry structure and electron density distribution in HOMO and LUMO. It is observed from the geometry optimized structure of inhibitor that it has non-planar in orientation. Thus, it is not adsorbed in a flat orientation on the mild steel surfaces. Thus the next question is obviously coming if molecule is not adsorbed in the flat mode then how incredible amount of inhibition efficiency has been shown by the particular inhibitor molecule. This issue can be addressed by the electron density distribution in FMO's of the inhibitor. The view of HOMO of the inhibitor revealed that electron density is distrusted over the 2-amino thiazol and oxime part of the molecule whereas; appreciable electron density is distributed in LUMO over the thiazine carboxylic acid part of the molecule. Therefore, a single molecule showed both type of behaviour; electron donation is due to one part of the molecule while electron donation by other part. This dual behaviour of molecule helps in adsorption of the inhibitor effectively. In this consequence, better inhibition efficiency is obtained by this particular inhibitor molecule.

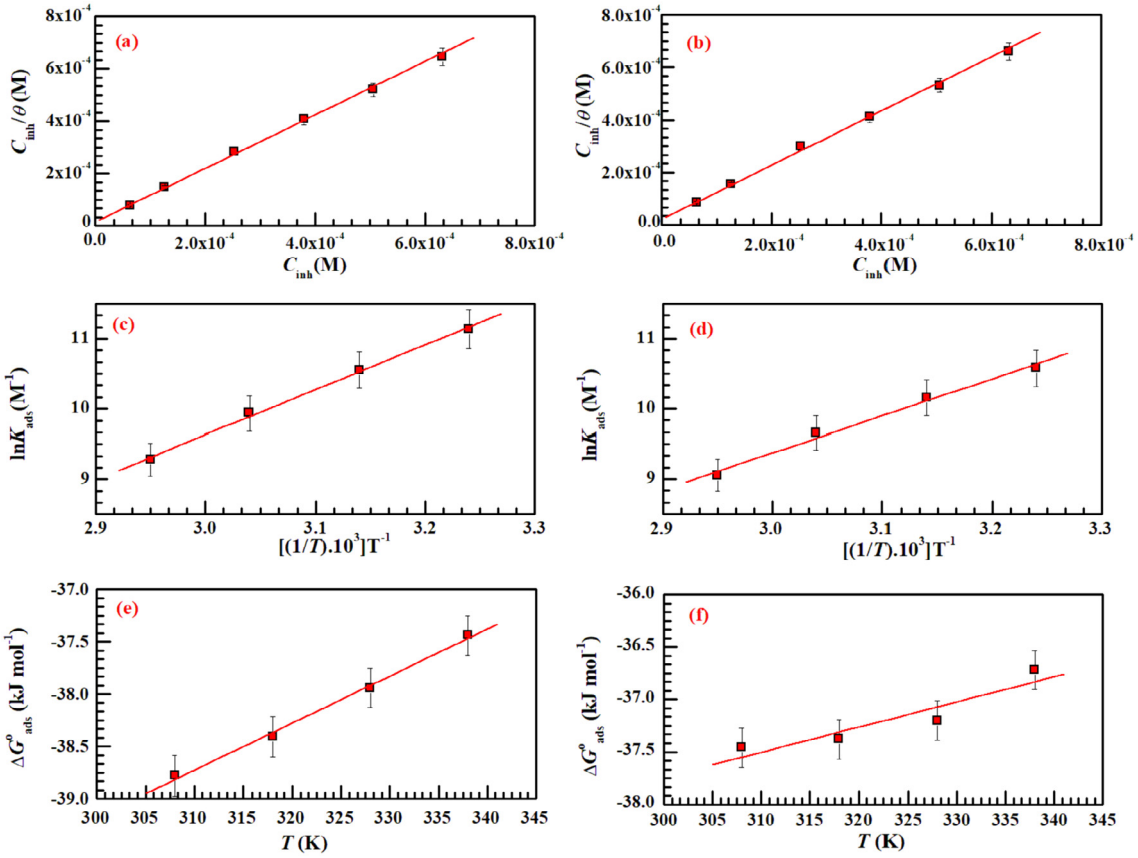

Fig. 6. (a) & (b) Langmuir adsorption isotherm plots, (c) & (d) plot of lnKadsvs 1/T and (e) & (f) *vs.* T obtained from weight loss and Tafel polarization method.

Table 7
Thermodynamic parameters of adsorption in presence of 5.05×10^{-4} M conc. of CDR.

Temperature (K)	K_{ads} ($10^4 \times M^{-1}$)		ΔG^o_{ads} (kJ mol^{-1})		ΔH^o_{ads} [a] (kJ mol^{-1})		ΔS^o_{ads} [a] (J mol^{-1}K^{-1})		ΔH^o_{ads} [b] (kJ mol^{-1})		ΔS^o_{ads} [b] (J mol^{-1}K^{-1})	
	WL	PDP	WL	PDP	WL	PDP	WL	PDP	WL	PDP	WL	PDP
308	6.86	3.92	38.78	37.46	−52.97	−43.37	45.44	18.76	52.60	−44.85	44.90	24.00
318	3.83	2.58	38.50	37.38								
328	2.07	1.56	38.04	37.20								
338	1.07	0.85	37.34	36.72								

[a] Calculated from Eq. (22).
[b] Calculated from Eq. (23).

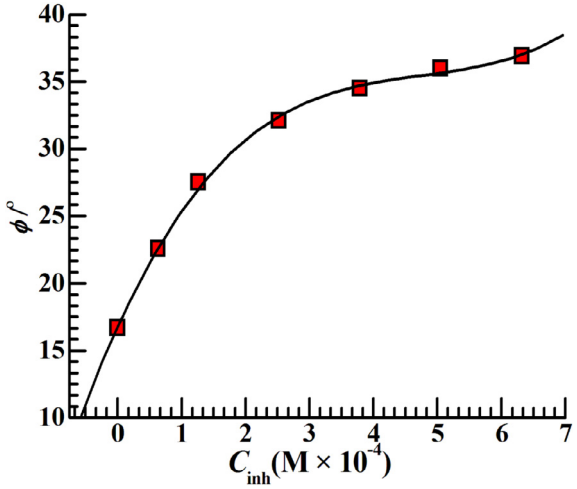

Fig. 7. Variation of contact angle, ϕ, with acid solutions containing varying concentrations of CDR on mild steel surface.

Inhibitor molecule adsorption can also be inferred by the energy of frontier molecular orbitals. The high value of E_{HOMO} and low value of E_{LUMO} ease the inhibitor adsorption as these values measure the tendency to donate and accept electrons [56–58]. It is seen from Table 8 that CDR inhibitor molecule has highest E_{HOMO} and lowest E_{LUMO} value in compared to some previously published molecules [59,60]. Apart from E_{HOMO} and E_{LUMO}, energy gap is another important parameter from where chemical reactivity of the molecule can be easily elucidate. As much as ΔE value decreases, there is an increase in its reactivity, which in turn increases the adsorption ability of the inhibitors [57,58]. Smaller ΔE (shown in Table 8) demonstrates that the molecule is much easier to be polarized and easily adsorbed on the mild steel surfaces.

In order to get further information, whether the inhibitor molecule capable enough to donate the electron or not, fraction of electron transferred (ΔY) between inhibitor molecule and metal surface is hereby calculated. The values of E_{HOMO} and E_{LUMO} can make calculation of a series of intrinsic molecular properties [61] *like* ionization potential (I), electron affinity (A), electronegativity (χ), global hardness (η) of the inhibitors. These parameters are related to each other by the following formula:

$$I = -E_{HOMO} \tag{24}$$

$$A = -E_{LUMO} \tag{25}$$

$$\chi = \frac{I + A}{2} \tag{26}$$

$$\eta = \frac{I - A}{2} \tag{27}$$

Pearson method [62] provides the calculation of fraction of electron transferred (ΔY) between inhibitor molecule and metal surface. According to this method, electrons flow towards high electronegativity

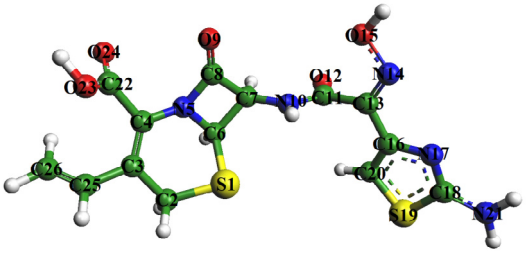

(a)

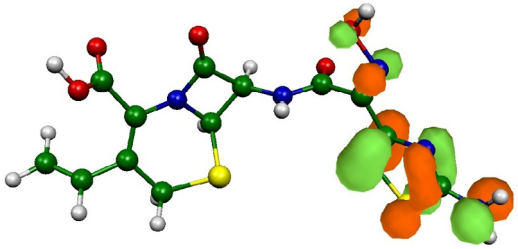

(b)

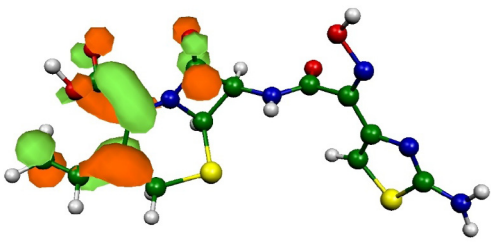

(c)

Fig. 8. (a) The optimized geometry, (b) HOMO and (c) LUMO of CDR molecule for neutral species in the aqueous phase.

Table 8
Calculated quantum chemical parameters of studied neutral form of CDR inhibitor.

Inhibitors	E_{HOMO} (eV)	E_{LUMO} (eV)	ΔE (eV)	μ (Debye)	$I = -E_{HOMO}$ $A = -E_{LUMO}$	χ	η	S	ΔY
CDR	−5.8961	−1.9039 3.9922	11.6625	5.8961	1.9039	3.9000	1.9961	0.5009	0.2304

from low electronegativity when system of different electronegativity comes in contact to each other. This flow continues till their chemical potential becomes equal. The ΔY value is calculated by the following equation [29,30]:

$$\Delta Y = \frac{\phi - \chi_{inh}}{2(\eta_{Fe} + \eta_{inh})} \quad (28)$$

where, ϕ, χ_{inh} stands for work function of iron and electronegativity of the inhibitor, while η_{Fe} and η_{inh} stands for hardness of Fe and inhibitor molecule, respectively.

The obtained DFT derived ϕ values for Fe (1 0 0), Fe (1 1 0) and Fe (1 1 1) surfaces are 3.91, 4.82 and 3.88 eV, respectively [29,35]. Herein, Fe (1 1 0) surface has been considered due to its packed surface and higher stabilization energy. Electrons transfer will occurs from inhibitor to metal surface atom when $\Delta Y > 0$ and *vice versa* [28–30]. Elnga *et al.* proposed that electron donation capability of inhibitor molecules when the ΔY value is less than 3.6 [63]. It can be seen from Table 8 that calculated ΔY value is positive and less than 3.6. Hence, inhibitor molecule is capable for electron donation to the metallic surface atom.

Another intrinsic molecular parameters which is associated to the chemical reactivity of the molecule is global softness (reciprocal of global harness, $1/\eta$). According to the HASB principle, inhibitor molecules are considered as soft bases and metals as soft acids [64]. Therefore, those inhibitor molecules which have higher softness value will easily adsorb on the metallic surfaces. Table 8 reveals that the obtained softness value of the studied inhibitor molecule is quite good enough in compared to some previously published molecules [65,66].

Quantum chemical calculations of the protonated form of inhibitor molecule

Presence of heteroatoms in the molecular scaffold of CDR molecule suggests their high possibility towards the protonation in the acidic medium. Therefore, it is essential to investigate how molecular property of the protonated form of inhibitor molecule play crucial role for the adsorption on the metallic surfaces. In this perspective, in order to find out the possible site of protonation, mulliken atomic charges of the neutral form of inhibitor molecule has been consider [67–69]. From Table 9 it is seen that, O12 atom possess highest negative charge. Thus, in the present investigation O12 atom is protonated. The optimized geometric configurations, HOMO and LUMO plot of the CDR molecule are shown in Fig. 9, whereas quantum chemical parameters obtained from DFT calculation (such as E_{HOMO}, E_{LUMO}, ΔE, μ, χ, η, S and ΔY) is tabulated in Table 10. From Table 10 it is seen that E_{HOMO} value of the inhibitor is shifted towards the more negative value in comparison to the E_{HOMO} value of neutral form. It suggest, in the protonated form electron donation capability of the CDR molecule decreases and it is also expected that in the protonation state inhibitor molecule is not quite capable enough to donate the electron. This finding is further counter supported by the fraction of electron transfer from the inhibitor to the metallic surface (ΔY). Table 10 reveals that ΔY obtained for protonation state of inhibitor molecule is negative. On the contrary, E_{LUMO} value tabulated in Table 10 also shifted towards the more negative value than that of neutral form, it pointing out electron acceptance capability in protonated form is increased. This is also counter supported by the electronegativity value of protonated form of inhibitor. If we compare electronegativity values of the neutral and protonated form of CDR molecule, it can be seen that electronegativity value in the protonated form of CDR molecules is much higher than that of the neutral form. It suggests electron attraction capability is better by the protonation form of inhibitor. Therefore, after successive analysis of both the neutral as well as protonation form of inhibitor molecule it can be concluded that neutral form of inhibitor have high tendency to donate electrons whereas protonation form inhibitor is much superior to accept electrons.

Table 9
DFT (ORCA) derived Mulliken atomic charges of the studied CDR molecule in neutral form.

Atoms	Mulliken atomic charge
S1	−0.002402
C2	−0.214226
C3	−0.039381
C4	0.198806
N5	−0.326403
C6	−0.004131
C7	0.092934
C8	0.268920
O9	−0.354757
N10	−0.333772
C11	0.291463
O12	−0.414719
C13	0.053952
N14	−0.253385
O15	−0.266988
C16	0.149620
N17	−0.390186
C18	0.148729
S19	0.104678
C20	−0.224276
N21	−0.341517
C22	0.127501
O23	−0.243463
O24	−0.327635
C25	−0.125003
C26	−0.199597

Active sites analysis of neutral form of molecule

The molecular behaviour of any molecule largely depends on geometry optimized structure and electron density distribution in FMO's. Although, a molecule may have number of active sites but it is quite essential to recognize which particular active sites of will principally participate in D-A type of interaction. Generally D-A type interactions resulted from electron rich heteroatoms [70]. Though, it is difficult to predict accurate point from where inhibitor molecule donate certain amount of charges through some centres and received significant amount of charges through the consecutive centres. This problem overcame by Fukui indices analysis which eases behavioural differentiation of different parts of molecule [71]. The value of f_x^+ and f_x^- decides the chemical behaviour of different part of a molecule. The atoms having high value of f_x^+ involve in the formation of back-bonding by accepting electrons from metal surface i.e. these atoms behave as electron deficient centres while atoms having sustainable f_x^-act as electron rich centres i.e. favours the formation of chemical bond through donation of electrons to vacant d-orbital of metal [57,72]. The Fukui indices calculated for all the atoms of CDR molecule are listed in Table 11. The Table 11 showed that S(1), C(3), C(4), C(8), O(9), C(22), O(23), O(24), C(25) and C(26) atoms of CDR molecule have high value of f_x^+ and hence are susceptible to accept electrons while N(14), O(15), C(16), N(17), C(18), S(19), C(20) and N(21) atoms having high value of

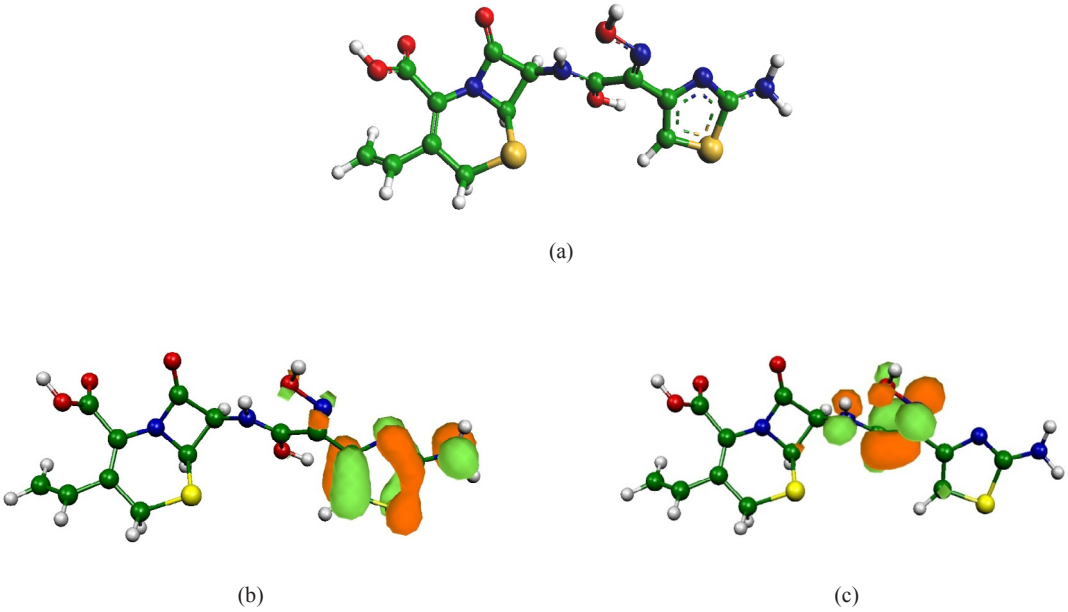

Fig. 9. (a) The optimized geometry, (b) HOMO and (c) LUMO of CDR molecule for protonated species in the aqueous phase.

$f_x^-$are involved in electron donation. Therefore, it is inferred that mainly thiazine carboxylic acid segment of the inhibitor molecule participated for accepting electrons, whereas 2-amino thiazol and oxime part of the CDR molecule for donating electrons. Thus it can be said conclusively that electron density distribution in FMO's and Fukui indices agreed well.

Molecular dynamics simulation

To understand interaction of inhibitor CDR with the Fe (1 1 0), MD simulation was carried out with consideration of all the concerned species (such as H_2O, H_3O^+, Cl^- and Fe surface) which are involved in the corrosion relate process. An appropriate and authentic configuration of surface adsorbed CDR molecule was obtained by means of MD simulation. The side and top view of the equilibrium adsorption configurations of surface adsorbed CDR are presented as Fig. 10a-b which elucidated that CDR molecule tend to acquire more or less planar orientation to favour its adsorption on the Fe (1 1 0) surface. This particular orientation provided maximum contact of CDR molecule with metal surface leaving minimum surface area to be attacked by aggressive corrosive species. Hence, superior inhibition effectiveness is expected and obtained accordingly.

Moreover, valuable information regarding adsorption potential of CDR is drawn from the values interaction energy (E_{inter}) or binding energy ($E_{binding}$). The interaction energy obtained for this system is presented in Table 12. The value of E_{inter} presented in Table 12 indicated a strong interaction of CDR molecule with the Fe (1 1 0) surface. Thus, it can be concluded that theoretical results agreed well with the experimental results.

Surface characterization: AFM study

The topographical analysis of mild steel electrodes was carried out by means of AFM. Atomic force microscope scanned the image of surface of different electrode sample which are presented as 3d images (Fig. 11a–c). The average surface roughness of studied sample prior to be immersed in an electrolytic solution was around 66 nm as presented by Fig. 11a. The average surface roughness got increased up to 395 nm (Fig. 11b) when the sample immersed in an electrolytic solution. The attack of acid solution to the mild steel surface was hindered when CDR

Table 11
Obtained Fukui indices for nucleophilic and electrophilic attack for CDR inhibitor molecule.

Atom	Fukui Indices for Nucleophilic Attack (f_x^+)	Fukui Indices for Electrophilic Attack (f_x^-)
S (1)	0.048	0.022
C (2)	0.020	0.004
C (3)	0.081	0.004
C (4)	0.061	0.004
N (5)	0.017	0.004
C (6)	0.010	0.003
C (7)	0.014	0.003
C (8)	0.050	0.003
O (9)	0.064	0.007
N (10)	0.004	0.005
C (11)	0.006	0.001
O (12)	0.016	0.020
C (13)	0.012	0.026
N (14)	0.020	0.067
O (15)	0.010	0.056
C (16)	0.006	0.071
N (17)	0.004	0.078
C (18)	0.004	0.056
S (19)	0.017	0.165
C (20)	0.012	0.103
N (21)	0.004	0.117
C (22)	0.060	0.001
O (23)	0.045	0.002
O (24)	0.084	0.003
C (25)	0.036	0.002
C (26)	0.082	0.006

Table 10
Calculated quantum chemical parameters of studied protonated form of CDR inhibitor.

Inhibitors	E_{HOMO} (eV)	E_{LUMO} (eV)	ΔE (eV)	M (Debye)	$I = -E_{HOMO}$	$A = -E_{LUMO}$	χ	η	S	ΔY
CDR	−6.3951	−3.4402	3.4647	10.51726	6.3951	3.4402	4.9176	1.4774	0.6768	−0.0330

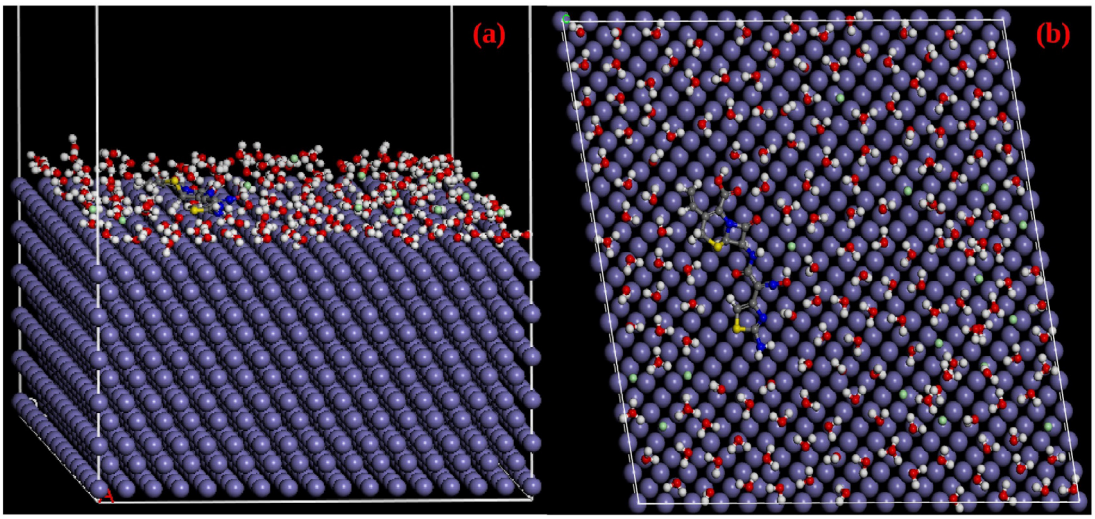

Fig. 10. Equilibrium adsorption configurations of CDR on Fe (1 1 0) surface obtained by MD simulations. (a): side view, (b): top view.

Table 12
Output obtained from MD simulation for adsorption of inhibitors on Fe (1 1 0) surface.

Systems	E_{inter} (kJ mol^{-1})	$E_{binding}$ (kJ mol^{-1})
Fe + CDR	−944.90	944.90

added to it which is supported by the fact that the average surface roughness reduced to 197 nm (Fig. 11c) compared to 395 nm.

Mechanism of corrosion inhibition

In general, adsorption plays an important role in corrosion inhibition by use of organic compounds as they get adsorbed and checked further corrosion. The results discussed so far supported this view in the case CDR also.

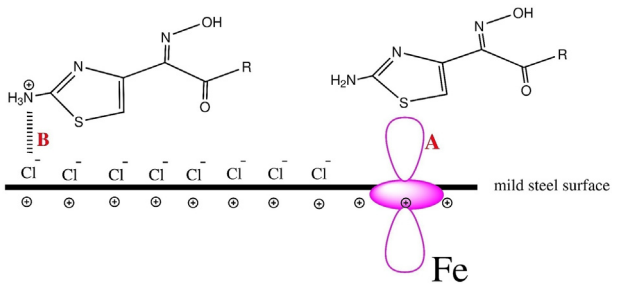

Fig. 12. Schematic representation of adsorption of CDR molecule on the mild steel surface (A) Chemisorption and (b) Electrostatic interaction.

A number of possible interactions through which CDR molecule can get adsorbed to the mild steel surface are presented by Fig. 12.

Generally inhibitors interact to metal surface in number of ways

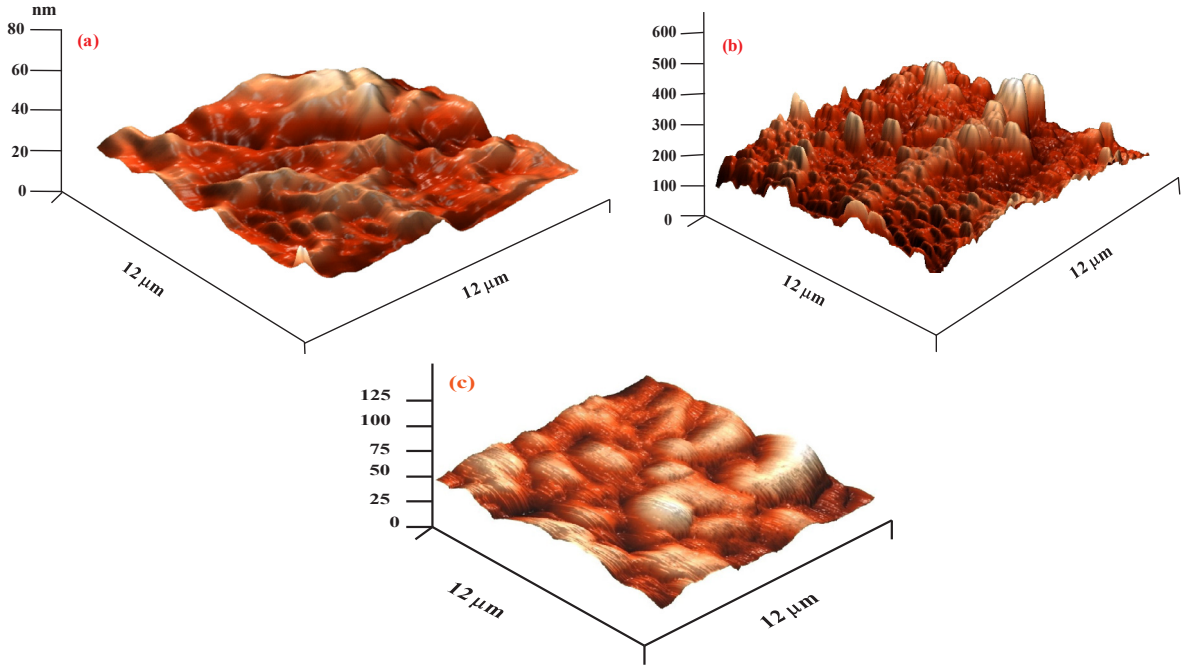

Fig. 11. Atomic Force Micrographs of (a) mild steel surface before immersion in HCl Solution, (b) After Immersion in 1 M HCl and (c) After immersion in HCl-CDR Solution.

[73–75] and thereby get adsorbed. They may interact through

(a) Electrostatic interaction which occur between differently charged objects, i.e. inhibitor molecule and metal surface,
(b) Non-bonded electrons of inhibitor to those metal orbitals which are vacant,
(c) Similarly unsaturation of inhibitor, i.e. π-electrons to vacant metal orbitals and
(d) Back-bonding or retro-donation. Inhibitor molecule and metal surface may interact in this way also.

Based on the above facts it can be understood that the deciding factors for adsorption and thereby corrosion inhibiting potential are molecular structure and electronic properties of the inhibitor molecule. It was observed that the inhibition potential of CDR decreases by increasing temperature at its smaller concentrations which attributed to electrostatic interaction. Further, when concentration of CDR increased, it showed appreciable efficiency against corrosion even at higher temperatures which might be due to change of interaction of CDR molecule to the metal surface on which it get adsorbed. The interaction of vacant 3d-orbitals of S-atom with 3delectrons of Fe assisted adsorption of CDR. The adsorption of CDR molecule is also aided by its π-electrons.

Conclusions

From all the facts discussed above following conclusions can be drawn

1. The Polarization study of CDR revealed its mixed type nature of inhibition. Also, cathodic part of polarization curves affected significantly by CDR.
2. The decreased value of contact angle by the presence of CDR confirmed the reduced affection of mild steel to the solution.
3. Langmuir isotherm can explained adsorption of CDR in best way.
4. The CDR molecule showed appreciable potential against mild steel corrosion at higher temperatures as confirmed by its thermal stability by TGA study.
5. The gravimetric as well as electrochemical results are well supported by AFM study.

Acknowledgement

Author AKS is thankful to Bharati Vidyapeeth's College of Engineering for providing a platform to carry out this research work. Author BC is thankful to NSIT for providing financial support as TRF to perform this research work. PB thanks Department of Higher Education, Science & Technology and Biotechnology (DHESTBT), Government of West Bengal for supporting research project [Ref. no. 78(Sanc.)/ST/P/S &T/6G-1/2018 and GAP-225612]. We are also thankful to our colleagues from respective Institution who assisted directly or indirectly for this research work. The authors are immensely grateful to reviewers for their comments that greatly improved the manuscript.

Declaration of Competing Interest

There are no conflicts to declare.

Appendix A. Supplementary data

Supplementary data to this article can be found online at https://doi.org/10.1016/j.rinp.2019.102383.

References

[1] Callister WD. Material Science and Engineering and Introduction. 4th ed. John Willy and sons Inc.; 1997. p. 550–4.
[2] Arshad N, Singh A, Chugh B, Akram M, Perveen F, Rasheed I, et al. Experimental, theoretical and surface study for corrosion inhibition of mild steel in 1 M HCl by using synthetic anti-biotic derivatives. Ionics 2019. https://doi.org/10.1007/s11581-019-03028-y.
[3] Obot IB, Umoren SA, Ankah NK. Pyrazine derivatives as green oil field corrosion inhibitors for steel. J Mol Liq 2019;277:749–61. https://doi.org/10.1016/j.molliq.2018.12.108.
[4] Xhanari K, Finsgar M. The first electrochemical and surface analysis of 2amino-benzimidazole as a corrosion inhibitor for copper in chloride solution. New J Chem 2017;41:7151–61. https://doi.org/10.1039/c7nj01209h.
[5] Prabakaran M, Kim SH, Sasireka A, Hemapriya V, Chung IM. β-Sitosterol isolated from rice hulls as an efficient corrosion inhibitor for mild steel in acidic environments. New J Chem 2017;41:3900–7. https://doi.org/10.1039/c6nj03760g.
[6] Singh AK, Thakur S, Pani B, Singh G. Green synthesis and corrosion inhibition study of 2-amino-: N ′-((thiophen-2-yl)methylene)benzohydrazide. New J Chem 2018;42:2113–24. https://doi.org/10.1039/c7nj04162d.
[7] Yıldız R. Adsorption and inhibition effect of 2, 4-diamino-6-hydroxypyrimidine for mild steel corrosion in HCl medium: experimental and theoretical investigation. Ionics 2019;25:859–70. https://doi.org/10.1007/s11581-018-2649-5.
[8] Zhang huan H, Pang X, Gao K. Localized CO_2 corrosion of carbon steel with different microstructures in brine solutions with an imidazoline-based inhibitor. Appl Surf Sci 2018;442:446–60. https://doi.org/10.1016/j.apsusc.2018.02.115.
[9] Guo L, Obot IB, Zheng X, Shen X, Qiang Y, Kaya S, et al. Theoretical insight into an empirical rule about organic corrosion inhibitors containing nitrogen, oxygen, and sulfur atoms. Appl Surf Sci 2017;406:301–6. https://doi.org/10.1016/j.apsusc.2017.02.134.
[10] Singh AK, Thakur S, Pani B, Chugh B, Lgaz H, Chung IM, et al. Solvent-free microwave assisted synthesis and corrosion inhibition study of a series of hydrazones derived from thiophene derivatives: experimental, surface and theoretical study. J Mol Liq 2019;283:788–803. https://doi.org/10.1016/j.molliq.2019.03.126.
[11] Kumar S. Eco-friendly corrosion inhibitors: Synergistic effect of ethanol extracts of calotropis for corrosion of mild steel in acid media using mass loss and thermometric technique at different temperatures. Prot Met Phys Chem Surfaces 2016;52:376–80. https://doi.org/10.1134/s2070205116020167.
[12] Chauhan DS, Ansari KR, Sorour AA, Quraishi MA, Lgaz H, Salghi R. Thiosemicarbazide and thiocarbohydrazide functionalized chitosan as ecofriendly corrosion inhibitors for carbon steel in hydrochloric acid solution. Int J Biol Macromol 2018;107:1747–57. https://doi.org/10.1016/j.ijbiomac.2017.10.050.
[13] Singh AK, Quraishi MA. Effect of Cefazolin on the corrosion of mild steel in HCl solution. Corros Sci 2010;52:152–60. https://doi.org/10.1016/j.corsci.2009.08.050.
[14] Shukla SK, Quraishi MA. Cefotaxime sodium: a new and efficient corrosion inhibitor for mild steel in hydrochloric acid solution. Corros Sci 2009;51:1007–11. https://doi.org/10.1016/j.corsci.2009.02.024.
[15] Shukla SK, Quraishi MA. The effects of pharmaceutically active compound doxycycline on the corrosion of mild steel in hydrochloric acid solution. Corros Sci 2010;52:314–21. https://doi.org/10.1016/j.corsci.2009.09.017.
[16] Shukla SK, Singh AK, Ahamad I, Quraishi MA. Streptomycin: a commercially available drug as corrosion inhibitor for mild steel in hydrochloric acid solution. Mater Lett 2009;63:819–22. https://doi.org/10.1016/j.matlet.2009.01.020.
[17] El-Naggar MM. Corrosion inhibition of mild steel in acidic medium by some sulfa drugs compounds. Corros Sci 2007;49:2226–36. https://doi.org/10.1016/j.corsci.2006.10.039.
[18] Shukla SK, Quraishi MA. Cefalexin drug: a new and efficient corrosion inhibitor for mild steel in hydrochloric acid solution. Mater Chem Phys 2010;120:142–7. https://doi.org/10.1016/j.matchemphys.2009.10.037.
[19] Singh AK, Quraishi MA. Adsorption properties and inhibition of mild steel corrosion in hydrochloric acid solution by ceftobiprole. J Appl Electrochem 2011;41:7–18. https://doi.org/10.1007/s10800-010-0202-y.
[20] Hameed RSA. Ranitidine drugs as non-toxic corrosion inhibitors for mild steel in hydrochloric acid medium. Port Electrochim Acta 2012;29:273–85. https://doi.org/10.4152/pea.201104273.
[21] Fouda AS, Mahmoud WM, Abdul Mageed HA. Evaluation of an expired nontoxic amlodipine besylate drug as a corrosion inhibitor for low-carbon steel in hydrochloric acid solutions. J Bio- Tribo-Corrosion 2016;2. https://doi.org/10.1007/s40735-016-0037-0.
[22] Al-Shafey HI, Abdel Hameed RS, Ali FA, Aboul-Magd AEAS, Salah M. Effect of expired drugs as corrosion inhibitors for carbon steel in 1M HCL solution. Int J Pharm Sci Rev Res 2014;27:146–52.
[23] Singh AK, Pandey AK, Banerjee P, Saha SK, Chugh B, Thakur S, et al. Eco-friendly disposal of expired anti-tuberculosis drug isoniazid and its role in the protection of metal. J Environ Chem Eng 2019;7:102971https://doi.org/10.1016/j.jece.2019.102971.
[24] Zarrouk A, Hammouti B, Dafali A, Bouachrine M, Zarrok H, Boukhris S, et al. A theoretical study on the inhibition efficiencies of some quinoxalines as corrosion inhibitors of copper in nitric acid. J Saudi Chem Soc 2014;18:450–5. https://doi.org/10.1016/j.jscs.2011.09.011.
[25] Neese F, Wennmohs F, Becker U, Bykov D, Ganyushin D, Hansen A, et al. An Ab Initio, DFT and Semiempirical SCF-MO Package, Version 2.9. Mulheim an der Ruhr, Germany: Max Planck Institute for Bioinorganic Chemistry; 2012.
[26] Lee C, Yang W, Parr RG. Development of the Colle-Salvetti correlation-energy formula into a functional of the electron density. Phys Rev B Condens Matter 1988;37:785–9. https://doi.org/10.1103/PhysRevB.37.785.
[27] Becke AD, Becke AD. Densityfunctionalthermochemistry III The role of exact exchange Density-functional thermochemistryIII. J Chem Phys 1993;98:5648–52. https://doi.org/10.1063/1.464913.

[28] Saha SK, Dutta A, Ghosh P, Sukul D, Banerjee P. Adsorption and corrosion inhibition effect of schiff base molecules on the mild steel surface in 1 M HCL medium: a combined experimental and theoretical approach. Phys Chem Chem Phys 2015;17:5679–90. https://doi.org/10.1039/c4cp05614k.

[29] Saha SK, Dutta A, Ghosh P, Sukul D, Banerjee P. Novel Schiff-base molecules as efficient corrosion inhibitors for mild steel surface in 1 M HCl medium: experimental and theoretical approach. Phys Chem Chem Phys 2016;18:17898–911. https://doi.org/10.1039/c6cp01993e.

[30] Saha SK, Murmu M, Murmu NC, Banerjee P. Evaluating electronic structure of quinazolinone and pyrimidinone molecules for its corrosion inhibition effectiveness on target specific mild steel in the acidic medium: a combined DFT and MD simulation study. J Mol Liq 2016;224:629–38. https://doi.org/10.1016/j.molliq.2016.09.110.

[31] Schäfer A, Huber C, Ahlrichs R. Fully optimized contracted Gaussian basis sets of triple zeta valence quality for atoms Li to Kr. J Chem Phys 1994;100:5829–35. https://doi.org/10.1063/1.467146.

[32] Mansfeld F. Tafel slopes and corrosion rates from polarization resistance measurements. Corrosion 1973;29:397–402. https://doi.org/10.5006/0010-9312-29.10.397.

[33] Standard practice for preparing, Cleaning, and Evaluating Corrosion Test Specimens (G 1-90) 16.

[34] Singh AK, Singh P. Adsorption behaviour of o-hydroxy acetophenone benzoyl hydrazone on mild steel/hydrochloric acid interface. J Ind Eng Chem 2015;21:552–60. https://doi.org/10.1016/j.jiec.2014.03.018.

[35] Materials Studio 6.1 Manual, Accelrys Inc., San Diego, CA, (2007).

[36] Tang Y, Xu J, Jing W, Lu G, Cang H, Cao Z. Novel benzimidazole derivatives as corrosion inhibitors of mild steel in the acidic media Part II: theoretical studies. Corros Sci 2014;83:292–8. https://doi.org/10.1016/j.corsci.2014.02.025.

[37] Ciezak JA, Trevino SF. Inelastic neutron scattering spectrum of cyclotrimethylenetrinitramine: a comparison with solid-state electronic structure calculations. J Phys Chem A 2006;110:5149–55. https://doi.org/10.1021/jp057098u.

[38] De Proft F, Martin JML, Geerlings P. Calculation of molecular electrostatic potentials and Fukui functions using density functional methods. Chem Phys Lett 1996;256:400–8. https://doi.org/10.1016/0009-2614(96)00469-1.

[39] Contreras RR, Fuentealba P, Galván M, Pérez P. A direct evaluation of regional Fukui functions in molecules. Chem Phys Lett 1999;304:405–13. https://doi.org/10.1016/S0009-2614(99)00325-5.

[40] Chakraborty T, Hens A, Kulashrestha S, Chandra Murmu N, Banerjee P. Calculation of diffusion coefficient of long chain molecules using molecular dynamics. Phys E Low-Dimensional Syst Nanostruct 2015;69:371–7. https://doi.org/10.1016/j.physe.2015.01.008.

[41] Sun H. COMPASS: an ab initio force-field optimized for condensed-phase applications overview with details on alkane and benzene compounds. J Phys Chem B 2002;102:7338–64. https://doi.org/10.1021/jp980939v.

[42] Sun H. The COMPASS force field: parameterization and validation for phosphazenes. Comput Theor Polym Sci 1998;8:229–46. https://doi.org/10.1016/S1089-3156(98)00042-7.

[43] Bunte SW, Sun H. Molecular modeling of energetic materials: the parameterization and validation of nitrate esters in the COMPASS force field. J Phys Chem B 2002;104:2477–89. https://doi.org/10.1021/jp991786u.

[44] Singh AK, Quraishi MA. The effect of some bis-thiadiazole derivatives on the corrosion of mild steel in hydrochloric acid. Corros Sci 2010;52:1373–85. https://doi.org/10.1016/j.corsci.2010.01.007.

[45] Toshima S, Uchida T. Specific adsorption of halide ions at the germanium electrolyte-solution interface; frequency dispersion of interfacial impedance. Electrochim Acta 1970;15:1717–32. https://doi.org/10.1016/0013-4686(70)80092-5.

[46] Wagner N, Gülzow E. Change of electrochemical impedance spectra (EIS) with time during CO-poisoning of the Pt-anode in a membrane fuel cell. J Power Sources 2004;127:341–7. https://doi.org/10.1016/j.jpowsour.2003.09.031.

[47] Singh AK. Inhibition of mild steel corrosion in hydrochloric acid solution by 3-(4-((Z)-indolin-3-ylideneamino)phenylimino)indolin-2-one. Ind Eng Chem Res 2012;51:3215–23. https://doi.org/10.1021/ie2020476.

[48] Riggs Jr. OL. Corrosion Inhibitors. 2nd ed. Houston, TX: C.C. Nathan; 1973.

[49] Li WH, He Q, Zhang ST, Pei CL, Hou BR. Some new triazole derivatives as inhibitors for mild steel corrosion in acidic medium. J Appl Electrochem 2008;38:289–95. https://doi.org/10.1007/s10800-007-9437-7.

[50] Obot IB, Gopiraman M, Kabanda MM, Adekunle AS, Ebenso EE, Ramaganthan B, et al. Synthesized photo-cross-linking chalcones as novel corrosion inhibitors for mild steel in acidic medium: experimental, quantum chemical and Monte Carlo simulation studies. RSC Adv 2015;5:76675–88. https://doi.org/10.1039/c5ra12097g.

[51] Singh P, Ebenso EE, Olasunkanmi LO, Obot IB, Quraishi MA. Electrochemical, theoretical, and surface morphological studies of corrosion inhibition effect of green naphthyridine derivatives on mild steel in hydrochloric acid. J Phys Chem C 2016;120:3408–19. https://doi.org/10.1021/acs.jpcc.5b11901.

[52] El Attari H, Lagrenée M, Jama C, Mernari B, Lebrini M, Traisnel M, et al. Corrosion control of mild steel using 3,5-bis(4-methoxyphenyl)-4-amino-1,2,4-triazole in normal hydrochloric acid medium. Corros Sci 2009;51:1628–35. https://doi.org/10.1016/j.corsci.2009.04.009.

[53] Gece G. The use of quantum chemical methods in corrosion inhibitor studies. Corros Sci 2008;50:2981–92. https://doi.org/10.1016/j.corsci.2008.08.043.

[54] Somasundaran P, Huang L. Adsorption/aggregation of surfactants and their mixtures at solid-liquid interfaces. Adv Colloid Interface Sci 2000;88:179–208. https://doi.org/10.1016/S0001-8686(00)00044-0.

[55] Solmaz R, Kardaş G, Çulha M, Yazici B, Erbil M. Investigation of adsorption and inhibitive effect of 2-mercaptothiazoline on corrosion of mild steel in hydrochloric acid media. Electrochim Acta 2008;53:5941–52. https://doi.org/10.1016/j.electacta.2008.03.055.

[56] Qussay A, Nassir MH, Kadhum AAH, Kadhim A, Mohamad AB, Gaaz TS, et al. Experimental and theoretical studies of benzoxazines corrosion inhibitors. Results Phys 2017;7:4013–9. https://doi.org/10.1016/j.rinp.2017.10.027.

[57] Verma C, Olasunkanmi LO, Ebenso EE, Quraishi MA, Obot IB. Adsorption behavior of glucosamine-based, pyrimidine-fused heterocycles as green corrosion inhibitors for mild steel: experimental and theoretical studies. J Phys Chem C 2016;120:11598–611. https://doi.org/10.1021/acs.jpcc.6b04429.

[58] Chen S, Zheng X, Xiang B, Zhang S, Qiang Y, Guo L. Experimental and theoretical studies of four allyl imidazolium-based ionic liquids as green inhibitors for copper corrosion in sulfuric acid. Corros Sci 2017;119:68–78. https://doi.org/10.1016/j.corsci.2017.02.021.

[59] Salarvand Z, Raeissi K, Meghdadi S, Talebian M, Amirnasr M. Enhanced Corrosion Resistance of Mild Steel in 1M HCl Solution by Trace Amount of 2-Phenyl-Benzothiazole Derivatives: Experimental, Quantum Chemical Calculations and Molecular Dynamics (MD) Simulation Studies Elsevier Ltd; 2016. https://doi.org/10.1016/j.corsci.2016.11.002.

[60] Haque J, Verma C, Srivastava V, Quraishi MA, Ebenso EE. Experimental and quantum chemical studies of functionalized tetrahydropyridines as corrosion inhibitors for mild steel in 1 M hydrochloric acid. Results Phys 2018;9:1481–93. https://doi.org/10.1016/j.rinp.2018.04.069.

[61] Lukovits I, Kálmán E, Zucchi F. Corrosion inhibitors – correlation between electronic structure and efficiency. Corrosion 2001;57:3–8. https://doi.org/10.5006/1.3290328.

[62] Martinez S. Inhibitory mechanism of mimosa tannin using molecular modeling and substitutional adsorption isotherms. Mater Chem Phys 2003;77:97–102. https://doi.org/10.1016/S0254-0584(01)00569-7.

[63] Awad MK, Mustafa MR, Elnga MMA. Computational simulation of the molecular structure of some triazoles as inhibitors for the corrosion of metal surface. J Mol Struct Theochem 2010;959:66–74. https://doi.org/10.1016/j.theochem.2010.08.008.

[64] Obot IB, Gasem ZM. Theoretical evaluation of corrosion inhibition performance of some pyrazine derivatives. Corros Sci 2014;83:359–66. https://doi.org/10.1016/j.corsci.2014.03.008.

[65] Deng S, Li X, Xie X. Hydroxymethyl urea and 1,3-bis(hydroxymethyl) urea as corrosion inhibitors for steel in HCl solution. Corros Sci 2014;80:276–89. https://doi.org/10.1016/j.corsci.2013.11.041.

[66] Yadav M, Sarkar TK, Obot IB. Carbohydrate compounds as green corrosion inhibitors: electrochemical, XPS, DFT and molecular dynamics simulation studies. RSC Adv 2016;6:110053–69. https://doi.org/10.1039/c6ra24026g.

[67] Kabanda MM, Murulana LC, Ozcan M, Karadag F, Dehri I, Obot IB, et al. Quantum chemical studies on the corrosion inhibition of mild steel by some triazoles and benzimidazole derivatives in acidic medium. Int J Electrochem Sci 2012;7:5035–56.

[68] Obi-Egbedi NO, Obot IB, El-Khaiary MI, Umoren SA, Ebenso EE. Computational simulation and statistical analysis on the relationship between corrosion inhibition efficiency and molecular structure of some phenanthroline derivatives on mild steel surface. Int J Electrochem Sci 2011;6:5649–75.

[69] Saha SK, Banerjee P. A theoretical approach to understand the inhibition mechanism of steel corrosion with two aminobenzonitrile inhibitors. RSC Adv 2015;5:71120–30.

[70] Bereket G, Hür E, Öretir C. Quantum chemical studies on some imidazole derivatives as corrosion inhibitors for iron in acidic medium. J Mol Struct Theochem 2002;578:79–88. https://doi.org/10.1016/S0166-1280(01)00684-4.

[71] Hegazy MA, Badawi AM. Abd El Rehim SS, Kamel WM. Corrosion inhibition of carbon steel using novel N-(2-(2-mercaptoacetoxy)ethyl)-N, N-dimethyl dodecan-1-aminium bromide during acid pickling. Corros Sci 2013;69:110–22. https://doi.org/10.1016/j.corsci.2012.11.031.

[72] Olasunkanmi LO, Obot IB, Kabanda MM, Ebenso EE. Some quinoxalin-6-yl derivatives as corrosion inhibitors for mild steel in hydrochloric acid: experimental and theoretical studies. J Phys Chem C 2015;119:16004–19. https://doi.org/10.1021/acs.jpcc.5b03285.

[73] Shokry H, Yuasa M, Sekine I, Issa RM, El-Baradie HY, Gomma GK. Corrosion inhibition of mild steel by Schiff base compounds in various aqueous solutions: part 1. Corros Sci 1998;40:2173–86. https://doi.org/10.1016/S0010-938X(98)00102-4.

[74] John S, Joseph B, Balakrishnan KV, Aravindakshan KK, Joseph A. Electrochemical and quantum chemical study of 4-[(E)-[(2,4-dihydroxy phenyl) methylidine] amino]-6-methyl-3-sulphanylidine-2,3,4,5-tetra hydro-1,2,4-triazin-5-one [DMSTT]. Mater Chem Phys 2010;123:218–24. https://doi.org/10.1016/j.matchemphys.2010.03.085.

[75] Dorantes H, Domínguez-Aguilar MA, Olivares-Xometl O, Arce E, Arellanes-Lozada P, Likhanova NV. Synthesis and corrosion inhibition of α-amino acids alkylamides for mild steel in acidic environment. Mater Chem Phys 2008;110:344–51. https://doi.org/10.1016/j.matchemphys.2008.02.010.